Desalination and Water Treatment
www.deswater.com
doi: 10.1080/19443994.2013.821029

52 (2014) 6598–6610
October

Taylor & Francis
Taylor & Francis Group

Performance of removal of salicylic acid residues from aqueous solution based on the magnetic TiO_2 nanocomposites

Wenli Zhang[a,*], Jiqin Li[a], Ziyang Lu[b], Yingying Luo[a], Fei Chen[c], Pengwei Huo[a], Jianming Pan[a], Yongsheng Yan[a]

[a]*School of Chemistry & Chemical Engineering, Jiangsu University, Jiangsu, Zhenjiang 212013, P.R. China*
Tel. +86 511 88790187; Fax: +86 511 88791108; email: luziyang126@126.com
[b]*School of the Environment, Jiangsu University, Jiangsu, Zhenjiang 212013, P.R. China*
[c]*School of Environmental Science & Engineering, Chang'an University, Shanxi, Xi'an 710054, P.R. China*

Received 17 April 2013; Accepted 11 June 2013

ABSTRACT

Magnetic TiO_2 nanocomposites with good monodispersity were successfully synthesized via a mild sol–gel method, which were used for removal of salicylic acid (SA) residues from aqueous solution. These as-prepared nanocomposites were extensively characterized by transmission electron microscopy, scanning electron microscope, N_2 adsorption–desorption isotherm with the Brunauer-Emmett-Teller method, Fourier-transformed infrared spectra, X-ray diffraction, and vibrating sample magnetometer. These results indicated that magnetic TiO_2 nanocomposites possessed the core-shell structure of good dispersibility, excellent chemical stability, and magnetic property (Ms = 22.11 emu/g). According to the results of series experiments, magnetic TiO_2 nanocomposites showed fast kinetics and satisfied adsorption capacity for adsorption of SA. Under the optimum experimental condition, the adsorption process followed pseudo-second-order reaction kinetics and Langmuir adsorption isotherm. Moreover, the thermodynamic parameters calculated from the adsorption data suggested that the adsorption of SA was a spontaneous and endothermic nature of the process. In addition, magnetic TiO_2 nanocomposites were proved to exhibit high catalytic efficiency for photodegradation of SA under visible light irradiation, and the intermediate products of photodegradation were inferred from the mass spectrometry.

Keywords: Adsorption; Isotherms; Kinetics; Magnetic TiO_2 nanocomposites; Photodegradation; Removal; Salicylic acid residues

1. Introduction

Salicylic acid (SA), known as o-hydroxy benzoic acid, is widely used as preservative, additive, and indicator and also a raw material for the synthesis of acetylsalicylic acid and its derivates [1–6]. Consequently, SA is frequently present in wastewaters originated in pharmaceutical, cosmetic and chemical industries [2–5]. The presence of SA in wastewater may cause the side effects on ecosystems and human health [5,6]. Therefore, the removal of SA from aquatic environment is an important topic in the field of environmental science and technology.

Currently, photocatalytic technology, as one green technology which uses the light energy to degrade

*Corresponding author.

pollutant, has attracted the attention of many researchers. Up to now, amongst various photocatalysts used for treatment, TiO_2 has shown excellent potential, with less preparation costs, long-term stability, and strong oxidizing power for the removal of unwanted organic pollutants [7–12].

However, the photocatalytic reaction needs the target pollutant to reach the surface of photocatalyst, hence adsorption plays a key role for the photocatalytic process. In other words, good adsorption promotes the target pollutants to come into contact with more photocatalytic active sites, leading to the better removal efficiency [13–15]. Traditionally, the high cost of nanocomposites has caused serious economical problems.

Consequently, interest has focused on the magnetic nanomaterials. Magnetic nanomaterials can make the separation process simple and fast, because it can be easily collected by a magnet without additional centrifugation or filtration, and maintains a very high recycling rate [16,17]. As one of the most widely used magnetic particles, iron oxide can be easily prepared. However, the low surface energy and easy aggregation of iron oxide nanospheres hinder their applications, and if TiO_2 is directly coated on the iron oxide nano-spheres, this will lead to the dissolution effect of light and reduce the efficiency of photocatalytic reaction. Therefore, in order to overcome the abovementioned drawbacks, the inert layer of SiO_2 between TiO_2 and the magnetic core was introduced, and this SiO_2 layer effectively solved this problem [18–20].

In the present work, the magnetic TiO_2 nanocomposites were prepared via a mild sol-gel method based on iron oxide as the magnetic core and SiO_2 as the inert layer. Furthermore, SA was chosen as the target pollutant. This research mainly focused on the design of magnetic TiO_2 nanocomposites and the behavior evaluation of removal of SA residues solution. The adsorption performance (containing adsorption parameters, equilibrium, kinetics, and thermodynamics) of magnetic TiO_2 nanocomposites towards SA was investigated. Moreover, the photocatalytic reaction (containing degradation rate (Dr), mineralization rate (Mr), and the intermediate products of photodegradation) of magnetic TiO_2 nanocomposites was also studied.

2. Experimental section

2.1. Chemicals and reagents

SA and tetraethyl orthosilicate (TEOS) (AR) were both obtained from Aladdin Reagent Co., Ltd. $FeCl_3{\cdot}6H_2O$ (AR), ethanol (AR), ethylene glycol (AR), sodium acetate (NaAc, AR), concentrated ammonia, and concentrated hydrochloric acid (37.8%) were all purchased from National Chemical Reagent Co., Ltd. Tetrabutyl titanate (CR) and polyethylene glycol 4,000 (PEG 4000) were from Sinopharm Chemical Reagent Co., Ltd. Deionized ultrapure water used in all experiments was purified with a Purelab Ultra (Organo, Tokyo, Japan).

2.2. Structural analysis

The morphology of magnetic TiO_2 nanocomposites was observed by a transmission electron microscope (TEM, JEOL, JEM-200CX) and a scanning electron microscopy (SEM, S-4800). The specific surface area was measured by using a NOVA 2000e analytical system (Quantachrome Co., USA). Fourier-transformed infrared (FT-IR) spectra were recorded on a Nicolet Nexus 470 FT-IR (Thermo Nicolet Co., USA) with 2.0 cm^{-1} resolution in the range 400–4,000 cm^{-1}, using KBr pellets. X-ray diffraction (XRD) analysis was used to characterize the crystal structure. XRD patterns were obtained with a D8 ADVANCE X-ray diffractometer (Bruker AXS Co., Germany). Magnetic measurement was carried out using a vibrating sample magnetometer VSM (7,300, Lakeshore) under a magnetic field up to 10 kOe. In this work, the degradation mechanism of tetracycline aqueous solution was detected by the Thermo LXQ mass spectrometry.

2.3. Preparation of magnetic TiO_2 nanocomposites

As the scheme of the synthesis approach shows in Fig. 1, iron oxide nanospheres were first prepared according to the literature [18]. Briefly, 5 mmol $FeCl_3{\cdot}6H_2O$ and 75 mL ethylene glycol were added into a dry beaker with magnetic agitation for 20 min at room temperature. Then, 44 mmol NaAc was dissolved in above solution with magnetic agitation. Afterwards, this mixture was transferred into a Teflon-lined stainlesssteel autoclave and sealed to heat at 473 K. After reaction for 16 h, the autoclave was cooled to room temperature. The black product was collected by a magnet and washed with ethanol for several times, and then dried at 323 K overnight.

In the following step, 5 mL TEOS and 36 mL alcohol were put into the flask with mechanical agitation for 15 min at 313 K, the mixed solution (contained 36 mL alcohol, 3 mL deionized water, and 10 mL concentrated ammonia) was then added into above flask drop by drop, this reaction was conducted under mechanical agitation for 30 min. Afterwards, 2 g of iron oxide was added into above mixture, this reaction was continued for another 6 h. Then, the product

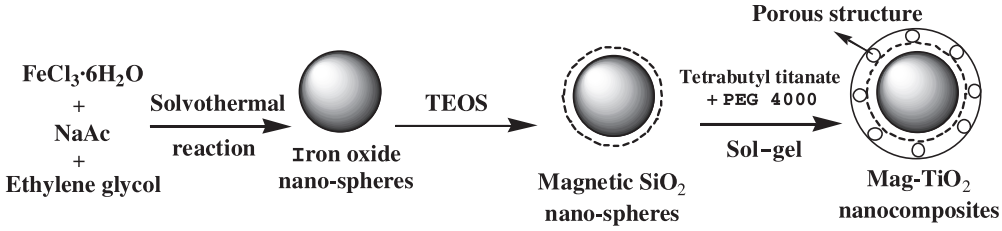

Fig. 1. Synthetic steps of mag-TiO_2 nanocomposites.

(collected by a magnet) was washed with deionized water and ethanol for several times, and dried 12 h at 323 K. Finally, the magnetic SiO_2 nanospheres were obtained.

The magnetic TiO_2 nanocomposites was prepared via the sol-gel method, the specific process was as follows: briefly, 0.0025 mmol PEG 4000, 10 mL tetrabutyl titanate and 36 mL alcohol were put into the flask with mechanical agitation for 15 min at 313 K. Subsequently, the mixed solution (contained 36 mL alcohol, 3 mL deionized water, and 0.2 mL concentrated hydrochloric acid) was added into above mixture drop by drop. When the sol was formed, 2 g magnetic SiO_2 nanospheres were added into the sol and kept stirring to the gel. After the gel was dried 12 h at 323 K and calcined 4 h at 773 K, the magnetic TiO_2 nanocomposites was obtained, hereinafter called mag-TiO_2 nanocomposites for short.

TiO_2/iron oxide was prepared using the same procedure of preparing mag-TiO_2 nanocomposites, in addition to using iron oxide nanospheres instead of magnetic SiO_2 nanospheres.

2.4. Batch mode adsorption studies

The experimental parameters on the adsorption of SA were studied in a batch mode of operations. A certain amount of mag-TiO_2 nanocomposites was dispersed in testing solution of SA (10 mL). After the desired time of static dark-adsorption at 303 K, the mag-TiO_2 nanocomposites were isolated by a magnet, and the concentration of SA in the solvent phase was determined with a UV-vis spectrophotometer. Moreover, the equilibrium adsorption capacity (Q_e, mg/g) was calculated according to Eq. (1):

$$Q_e = \frac{(C_0 - C_e)V}{W} \quad (1)$$

(C_0 (mg/L) and C_e (mg/L) are the initial and equilibrium concentrations of SA, respectively. V (mL) is the volume of testing solution and W (g) is weight of mag-TiO_2 nanocomposites.)

2.5. Photocatalytic degradation activity experiment

The photodegradation reaction was conducted in a dark closed photocatalytic reactor at 303 K and initiated by irradiating with two 150 W tungsten lamp with a light intensity of 390 mW/cm^2 determined with a CEL-NP 2000 light power meter (Beijing ZJJY Technology Co. Ltd.). The reaction flask contained 0.2 g mag-TiO_2 nanocomposites and 50 mL 20 mg/L SA aqueous solution. The sample analysis was conducted in the interval of 5 min, and the concentration of SA was analyzed by with a UV-vis spectrophotometer (UV2450, Shimadzu, Japan). The degradation rate (Dr) was calculated by Eq. (2). The mineralization of SA was determined by total organic carbon (TOC) value which was obtained by a TOC analyzer (Multi N/C 2100, Analytik jena AG, Germany). The mineralization rate (Mr) was calculated by Eq. (3):

$$\mathrm{Dr} = \left(1 - \frac{C}{C_0}\right) \times 100\% \quad (2)$$

where C_0 is the initial concentration; C is the concentration of the reaction solution.

$$\mathrm{Mr} = \left(1 - \frac{T}{T_0}\right) \times 100\% \quad (3)$$

where T_0 is the organic carbon content of the initial solution; T is the organic carbon content of the reaction solution.

3. Results and discussion

3.1. Characterization of mag-TiO_2 nanocomposites

The morphology of mag-TiO_2 nanocomposites was observed by TEM and SEM, which are shown in Figs. 2 and 3. As can be observed in Figs. 2(b) and Fig. 3, after coating SiO_2 inert layer and TiO_2 layer, the shape of mag-TiO_2 nanocomposites was still kept spherical and had good dispersibility, the mean diameter of mag-TiO_2 nanocomposites was near 290 nm. Furthermore, the core-shell structure could

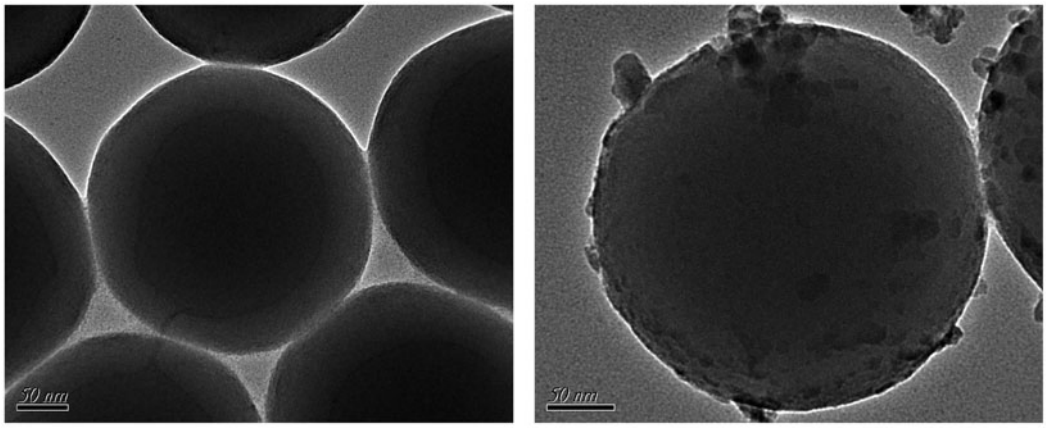

Fig. 2. TEM images of magnetic SiO_2 nanospheres (a), mag-TiO_2 nanocomposites (b).

be clearly seen in Fig. 2(a), dark part was core (iron oxide) and bright part was shell (SiO_2); the core diameter and shell thickness was approximately 130 nm and 50 nm, respectively. The N_2 adsorption–desorption isotherm and corresponding pore size distribution of the as-prepared mag-TiO_2 nanocomposites are shown in Fig. 4. It could be clearly seen that the material possessed of typical IV isotherm and the pore size distribution exhibited a sharp peak centered at 5.6 nm, which was attributed to the calcinations of PEG 4000.

Fig. 5 shows the XRD patterns; it could be clearly seen that the two patterns of iron oxide nanospheres and magnetic SiO_2 nanopheres were nearly the same. However, the SiO_2 inert layer was clearly seen in Fig. 2(a), illustrating that the SiO_2 inert layer was amorphous. The diffraction peaks of anatase TiO_2 ($2\theta = 25.5^\circ$, 37°, 48.1°, 54.4°, 63.2°) [21] appeared in the pattern of mag-TiO_2 nanocomposites, suggesting that mag-TiO_2 nanocomposites possessed the crystalline structure of anatase TiO_2. In addition, the elements of silicon and titanium displayed in Fig. 3(b) (EDS image) also proved that the SiO_2 inert layer and TiO_2 were successfully coated on the magnetic core (iron oxide).

The FT-IR spectra of TiO_2/iron oxide and mag-TiO_2 nanocomposites were measured by using KBr disks and are shown in Fig. 6. As shown in Fig. 6, in addition to the peak at 1,093 cm^{-1}, the two curves were almost the same. For the mag-TiO_2 nanocomposites, near 1,093 cm^{-1} was the stretching of Si–O–Si peak, which illustrated that the SiO_2 inert layer was successfully coated on the surface of magnetic core (iron oxide). Furthermore, the stretching band at 1,630 cm^{-1} may be attributed to the presence of residual physisorbed water molecules [22]. And due to the process of high-temperature calcination, PEG 4000 was removed from the system, thus there are no other absorption peaks in the two curves.

Fig. 7 shows the magnetic hysteresis loop of mag-TiO_2 nanocomposites and the magnetic separation ability was tested in aqueous solution by placing a magnet near the centrifuge tube (inset). The general shape and trend of the curve showed that mag-TiO_2 nanocomposites possessed good magnetic property. However, the magnetization saturation (Ms) value of mag-TiO_2 nanocomposites (22.11 emu/g) was lower than that of Fe_3O_4; this was because the mass percent of iron, silicon, and titanium in the mag-TiO_2 nanocomposites was 41.53, 17.99, and 40.48%, respectively (calculated from section 2.3). Moreover, the photograph (inset) also demonstrated that the mag-TiO_2 nanocomposites could be easily separated from the aqueous solution by a magnet.

3.2. Influence of analyte dose on adsorption of SA

As we know, the analyte dose played a key role in the adsorption process. Therefore, the influence of analyte dose was investigated in this part, which is shown in Fig. 8. In the present investigation, the temperature was chosen at 303 K, and the adsorption of 10 mL 20 mg/L SA for 8 h was studied during the analyte dose range of 0.0025 g–0.1 g. In order to obtain a good adsorption, both the bigger equilibrium adsorption capacity (Q_e) and the higher removal efficiency were needed. From Fig. 8, it could be clearly seen that the two curves crossed at the point of

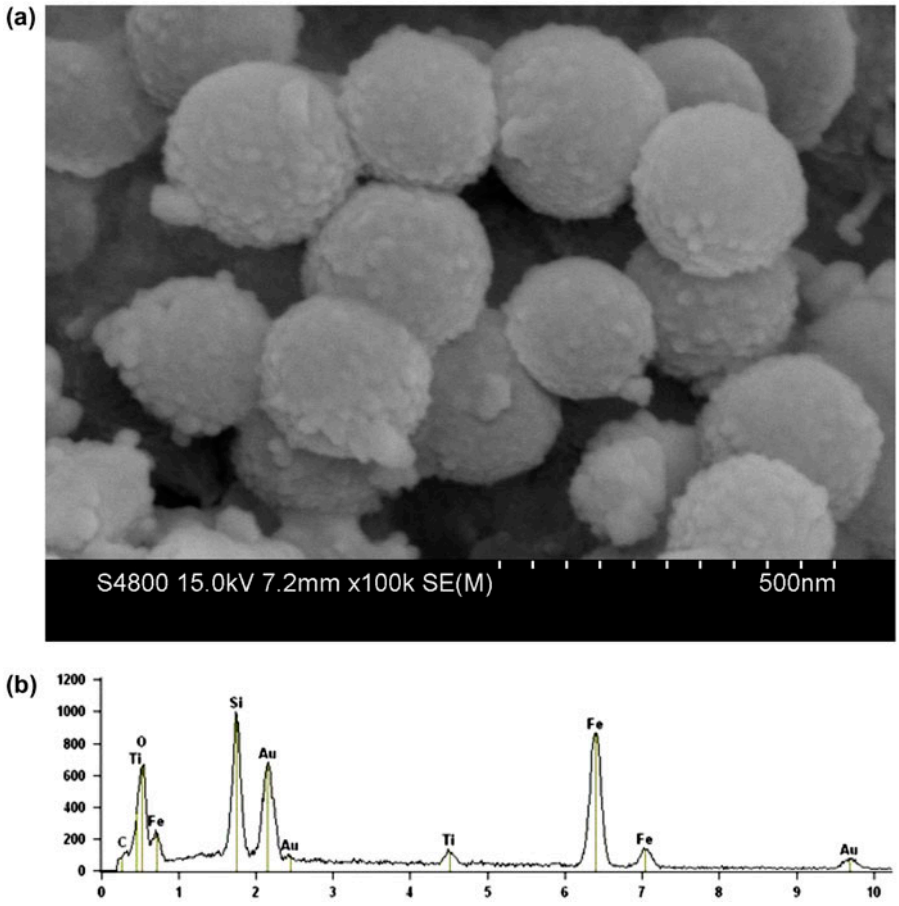

Fig. 3. SEM image of mag-TiO_2 nanocomposites (a), EDS of mag-TiO_2 nanocomposites (b).

0.02 g, in other words, when 0.02 g was chosen as the analyte dose, the adsorption of SA for 8 h under 303 K had both the bigger Q_e and the higher removal efficiency than others. Therefore, at the following experiments, 0.02 g as the analyte dose was chosen to use.

3.3. Adsorption isotherm

Adsorption isotherm model was very important to investigate how SA interacted with mag-TiO_2 nanocomposites. The equilibrium data of mag-TiO_2 nanocomposites was then fitted to the Langmuir and Freundlich isotherm models. The applicability of the isotherm models to the adsorption behaviors was studied by judging the correlation coefficient (R^2). The adsorption isotherm constants for mag-TiO_2 nanocomposites at different temperatures are listed in Table 1. Moreover, the comparison of Langmuir and Freundlich isotherm models for SA adsorption onto mag-TiO_2 nanocomposites using curve fitting are also illustrated in Fig. 9.

The Langmuir isotherm model assumed the uniform adsorption on the surface and the monolayer sorption with a homogenous distribution of sorption sites and sorption energies. The linear form and nonlinear form were expressed by the following equation, respectively [23]:

$$\frac{C_e}{Q_e} = \frac{1}{Q_m K_L} + \frac{C_e}{Q_m} \tag{4}$$

$$Q_e = \frac{K_L Q_m C_e}{1 + K_L C_e} \tag{5}$$

where C_e is the equilibrium concentration of SA (mg/L), Q_e is the equilibrium adsorption capacity (mg/g), Q_m is the maximum adsorption capacity, and K_L represents the affinity constant.

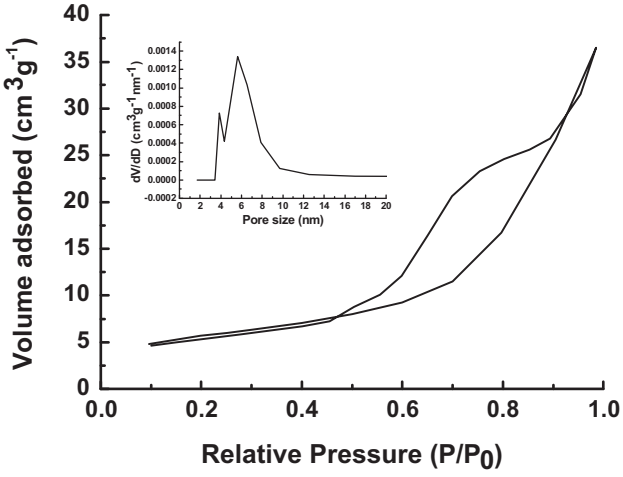

Fig. 4. N_2 adsorption–desorption isotherms and corresponding pore size distribution curve (inset) of mag-TiO_2 nanocomposites.

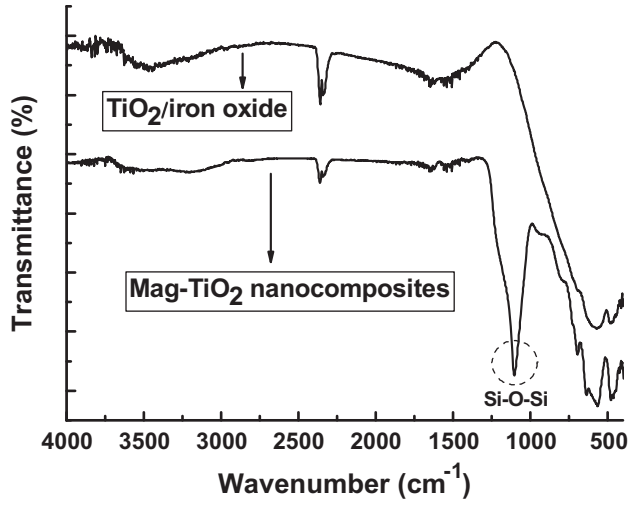

Fig. 6. FT-IR spectra of TiO_2/iron oxide and mag-TiO_2 nanocomposites.

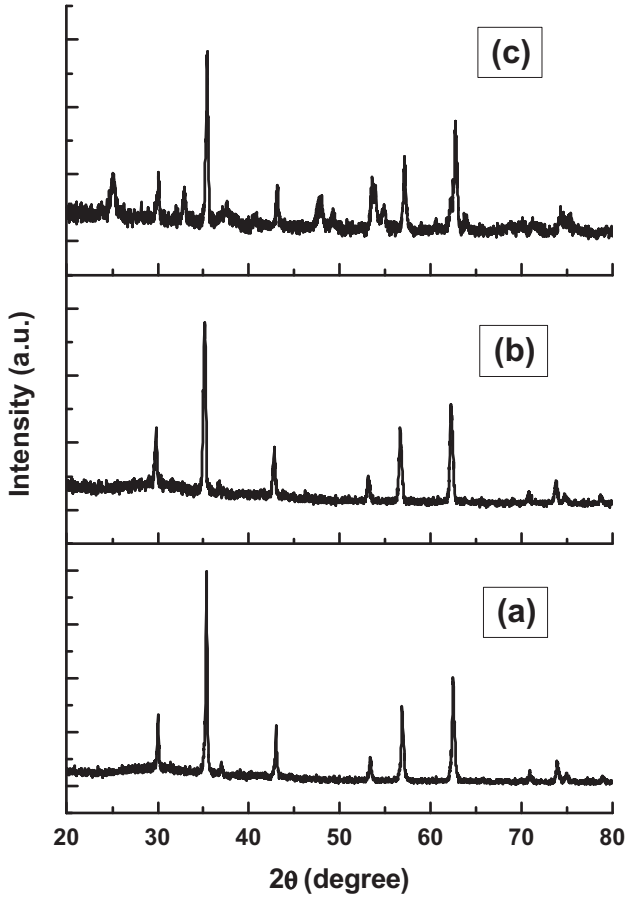

Fig. 5. The XRD patterns of iron oxide nanospheres (a), magnetic SiO_2 nanospheres (b) and mag-TiO_2 nanocomposites (c).

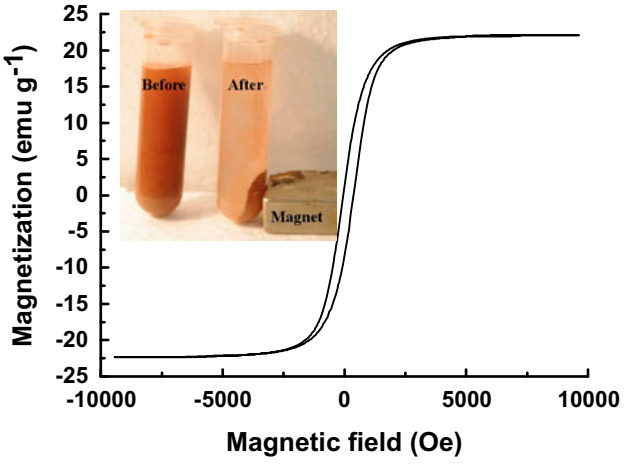

Fig. 7. Magnetization curve of mag-TiO_2 nanocomposites at room temperature and the inset in it: mag-TiO_2 nanocomposites separated from the aqueous solution by a magnet.

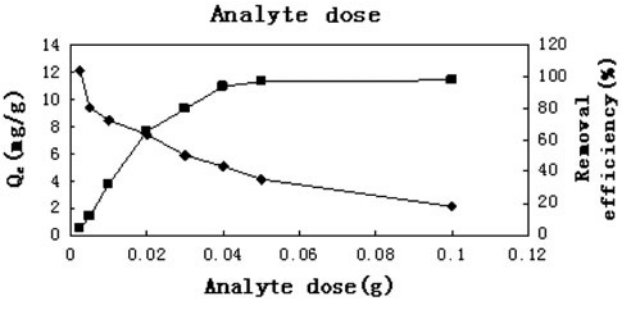

Fig. 8. Influence of analyte dose on adsorption of SA.

Table 1
Adsorption isotherm constants for mag-TiO_2 nanocomposites

Adsorption isotherm models	Constants	Mag-TiO_2 nanocomposites		
		303 K	313 K	323 K
Langmuir equation	R^2	0.9997	0.9993	0.9992
	$Q_{m,c}$ (mg/g)	9.6899	11.9474	12.2249
	K_L (L/mg)	0.2128	0.1944	0.3432
	R_L	0.0629	0.0685	0.0399
Freundlich equation	R^2	0.9029	0.9245	0.9479
	K_F (mg/g)	2.9675	3.2568	4.6144
	n	3.3300	2.9940	3.8417

Note: Analyte dose: 0.02 g, solution volume: 10 mL, contact time: 8 h, temperature of medium: 303, 313 and 323 K.

For predicting the favorability of an adsorption system, the Langmuir equation can also be expressed in terms of a dimensionless separation factor R_L defined as follow [24]:

$$R_L = \frac{1}{1 + C_m K_L} \tag{6}$$

where C_m is the maximal initial concentration of SA, R_L indicates the favorability and the capacity of adsorption system, If $R_L > 1$, the isotherm is unfavorable; $R_L = 1$, the isotherm is linear; $0 < R_L < 1$, the isotherm is favorable; $R_L = 0$, the isotherm is irreversible.

The linear and nonlinear forms of the Freundlich isotherm model were given as follows [25]:

$$\ln Q_e = \ln K_F + (1/n) \ln C_e \tag{7}$$

$$Q_e = K_F C_e^{(1/n)} \tag{8}$$

where K_F is an indicative constant for adsorption capacity (mg/g) and $1/n$ indicates the intensity of the adsorption. Value of $n > 1$ represents a favorable adsorption condition [26].

From Table 1 and Fig. 9, the mag-TiO_2 nanocomposites had good applicability to Langmuir isotherm, indicating that the adsorption of SA onto mag-TiO_2 nanocomposites was the monolayer adsorption.

3.4. Adsorption kinetics

In order to examine the controlling mechanism of adsorption process (such as mass transfer and chemical reaction), the kinetic data obtained have been analyzed using pseudo-first-order rate equation and pseudo-second-order rate equation. The pseudo-first-order equation can be expressed as [27]:

$$\ln(Q_e - Q_t) = \ln Q_e - K_1 t \tag{9}$$

$$Q_t = Q_e - Q_e e^{-K_1 t} \tag{10}$$

where Q_e and Q_t are the amount of SA (mg/g) onto mag-TiO_2 nanocomposites at the equilibrium and at time t (min), respectively, and k_1 (L/min) is the rate constant of pseudo-first-order adsorption.

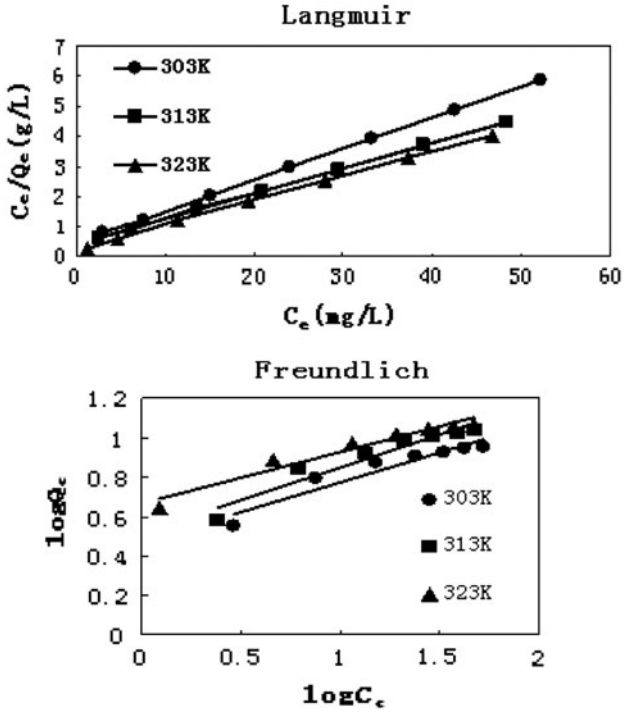

Fig. 9. Comparison of Langmuir and Freundlich isotherm models for SA adsorption onto mag-TiO_2 nanocomposites using curve fitting. Analyte dose: 0.02 g, solution volume: 10 mL, contact time: 8 h, temperature of medium: 303, 313 K and 323 K.

Table 2
Kinetic constants for the pseudo-first-order equation and pseudo-second-order equation

Adsorbate	C_0 (mg/L)	T (K)	$Q_{e,exp}$ (mg/g)	Pseudo-first-order equation			Pseudo-second-order equation			
				$Q_{e,c}$ (mg/g)	K_1 (L/min)	R^2	$Q_{e,c}$ (mg/g)	K_2 (g/mg·min)	h (mg/g·min)	R^2
SA	20	303	6.2300	4.1417	0.8929	0.9619	6.4433	0.0100	0.4152	0.9998
		313	6.9200	4.9229	0.8882	0.9526	7.1429	0.0088	0.4490	0.9997
	30	303	7.4500	4.9121	0.8936	0.8702	7.5815	0.0109	0.6265	0.9998

Note: Analyte dose: 0.02 g; solution volume: 10 mL, contact time: 8 h.

The second pseudo-second-order equation can be expressed as [28,29]:

$$\frac{t}{Q_t} = \frac{1}{K_2 Q_e^2} + \frac{t}{Q_e} \tag{11}$$

$$Q_t = \frac{K_2 Q_e^2 t}{1 + K_2 Q_e t} \tag{12}$$

$$h = K_2 Q_e^2 \tag{13}$$

where Q_e and Q_t are the amount of SA (mg/g) onto mag-TiO_2 nanocomposites at the equilibrium and at time t (min), respectively, k_2 (g/mg·min) is the rate constant of pseudo-second-order adsorption, and h (mmol/g·min) is the initial adsorption rate of pseudo-second-order model.

The adsorption rate constants and regression values are summarized in Table 2. The curve fitting plots of pseudo-first-order and pseudo-second-order kinetic model are shown in Fig. 10. It could be observed that the adsorption of SA followed the pseudo-second-order kinetics well because of the favorable fit between experimental and calculated data of equilibrium adsorption capacity (Q_e) (R_2 values above 0.9997), indicating that the chemical process was the rate-limiting step in the adsorption process [30]. According to the results, with the increase of initial concentration, the initial adsorption rate and adsorption capacity increased obviously. It was possible because the initial concentrations of SA provided the necessary driving force to overcome the resistances of mass transfer between the aqueous phases and the solid phase [31].

3.5. Adsorption thermodynamics

The sorption thermodynamics were necessary to be considered because they could conclude whether the process was spontaneous or not and gained an insight into the sorption behavior. Parameters including Gibbs free energy change (ΔG^o), enthalpy change (ΔH^o), and entropy change (ΔS^o) were calculated according to the following thermodynamic equations [32]:

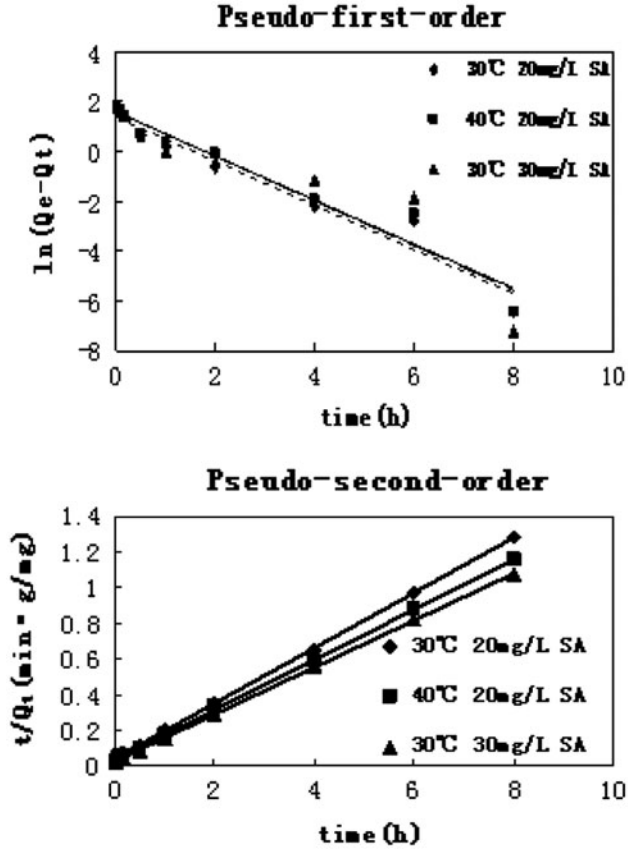

Fig. 10. Kinetic modeling of the effect of initial concentration and temperature on adsorption of SA onto mag-TiO_2 nanocomposites: Analyte dose: 0.02 g, solution volume: 10 mL, contact time: 8 h, temperature of medium: 303 and 313 K, initial concentration of SA: 20 and 30 mg/L.

Table 3
Thermodynamic parameters for the adsorption of SA onto mag-TiO_2 nanocomposites

Analyte	T (K)	Thermodynamic parameters		
		ΔG° (kJ/mol)	ΔH° (kJ/mol)	ΔS° (J/mol K)
mag-TiO_2 nanocomposites	303	−25.9185	19.74	0.1497
	313	−26.5379		
	323	−28.9129		

Note: Analyte dose: 0.02 g; solution volume: 10 mL; contact time: 8 h.

$$\ln\left(\frac{Q_e}{C_e}\right) = \frac{\Delta S^\circ}{R} - \frac{\Delta H^\circ}{RT} \quad (14)$$

$$\Delta G^\circ = \Delta H^\circ - T\Delta S^\circ \quad (15)$$

where R is the gas constant (8.314 J/mol K) and T is the absolute temperature (K).

The obtained thermodynamic parameters are listed in Table 3. A negative ΔG^o value indicated that the nature of adsorption of SA was spontaneous and more favorable at higher temperature. Moreover, the positive values of enthalpy change ΔH^o further confirmed the endothermic nature of the processes, Fig. 11 also proved this view. In addition, by adsorption of SA on the surface of mag-TiO_2 nanocomposites, the number of the water molecules surrounding SA molecules decreased and the degree of the freedom of the water molecules increased. Therefore, the positive values of ΔS^o suggested increased randomness at the solid–solution interface in the process of adsorption of SA on the surface of mag-TiO_2 nanocomposites [33].

3.6. Photocatalytic activity

Adsorption is a very important factor to photocatalysis, because the photocatalytic reaction needs the target pollutant to reach the surface of the photocatalyst. In order to prove that the mag-TiO_2 nanocomposites we prepared have a good photocatalytic activity, two groups of photocatalyst were studied, which is shown in Fig. 12(a). It could be clearly seen that the degradation rate of mag-TiO_2 nanocomposites could reach nearly 78% for photodegradation of 50 mL 20 mg/L SA in 30 min under the visible light irradiation, which was higher than that of TiO_2/iron oxide (65%). This demonstrated that the introduction of SiO_2 inert layer effectively solved the problem of the light dissolution effect, and the mag-TiO_2 nanocomposites possessed the strong ability to degrade SA residues from aqueous solution.

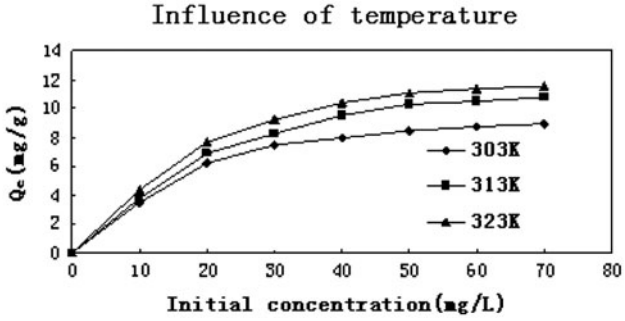

Fig. 11. Influence of temperature.

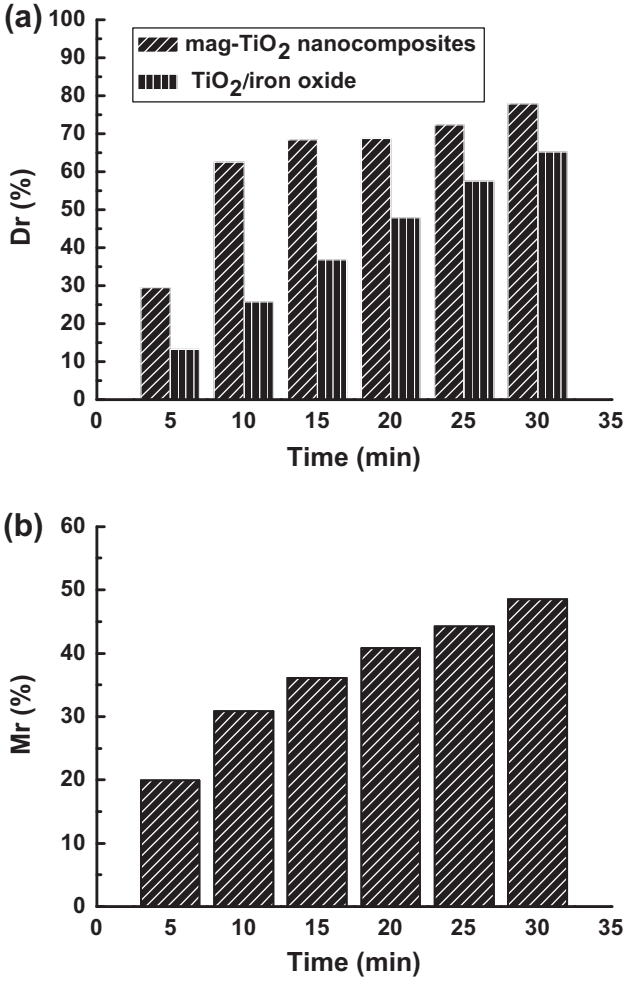

Fig. 12. The photocatalytic activity ((a). the degradation rate with different photocatalysts, (b). the mineralization rate with mag-TiO_2 nanocomposites).

In addition, the mineralization of SA was quantified by measuring the TOC content of the solution with the results summarized in Fig. 12(b). TOC analysis demonstrated that about 49% SA had been

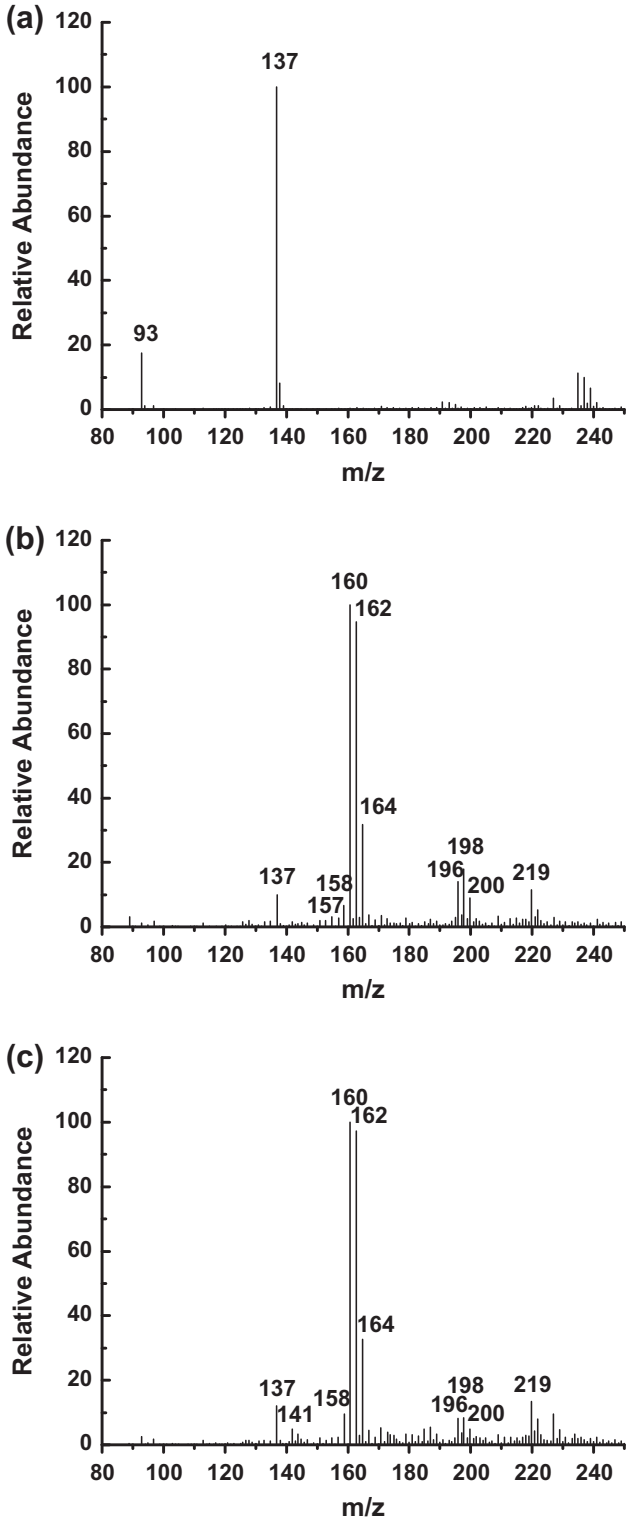

Fig. 13. m/z of degraded SA ((a). the initial SA solution, (b). photodegradation of SA in 15 min, (c). photodegradation of SA in 30 min).

disintegrated into CO_2 and H_2O over mag-TiO_2 nanocomposites after visible light irradiation for 30 min. Overall, the mineralization rate was significantly lower than the degradation rate, indicating that there were a lot of intermediates produced during the photocatalytic process.

According to the experimental results, we proposed the possible mechanism of photodegradation of SA with mag-TiO_2 nanocomposites; MS was employed to identify the intermediates, which was shown in Fig. 13. It could be found that there were many intermediates generated in Fig. 13(b) and (c), the mass measurement (m/z) of photodegradation of SA was presented in Table 4. From Fig. 13 and Table 4, it could be seen that the measured mass ($m/z = 93$) was found in Fig. 13(a), illustrating that the initial SA solution contained impurity.

In addition, the intermediate products of photodegradation of SA with mag-TiO_2 nanocomposites were inferred from the MS, the results are shown in Fig. 14. In process Ⅰ, B ($m/z = 256$) was obtained by the esterification of A ($m/z = 137$), then by losses of −OH and −COOH, C ($m/z = 196$) was generated, and D ($m/z = 198$) was transformed from C ($m/z = 196$). In process Ⅱ, E ($m/z = 93$) was generated from A ($m/z = 137$) by loss of −COOH, and F ($m/z = 100$) was obtained from E ($m/z = 93$) by the addition reaction of hydrogen, then with the esterification of F ($m/z = 100$), G ($m/z = 219$) was generated, H ($m/z = 226$) was also obtained from G ($m/z = 219$) by the addition reaction of hydrogen; afterwards, H ($m/z = 226$) was fragmented into I ($m/z = 224$), and I ($m/z = 224$) was further fragmented into J ($m/z = 200$, by loss of $-C_2H_2$) and K ($m/z = 196$, by loss of −C=O) and L ($m/z = 198$) was obtained from K ($m/z = 196$) by the addition reaction of hydrogen. In process III, E ($m/z = 93$) was attacked by the active species (·OH radical),

Table 4
Mass measurement for photodegradation of SA with mag-TiO_2 nanocomposites

	Measured mass (m/z)
The SA solution	93, 137
Photodegradation of SA in 15 min	137↓, 157↑, 158↑, 160↑, 162↑, 164↑, 196↑, 198↑, 200↑, 219↑
Photodegradation of SA in 30 min	137, 141↑, 158, 160↑, 162, 164, 196↓, 198↓, 200↓, 219

Note: The changes in measured mass was marked with ↑ and ↓ (↑ indicating the measured mass increased, ↓ indicating the measured mass decreased).

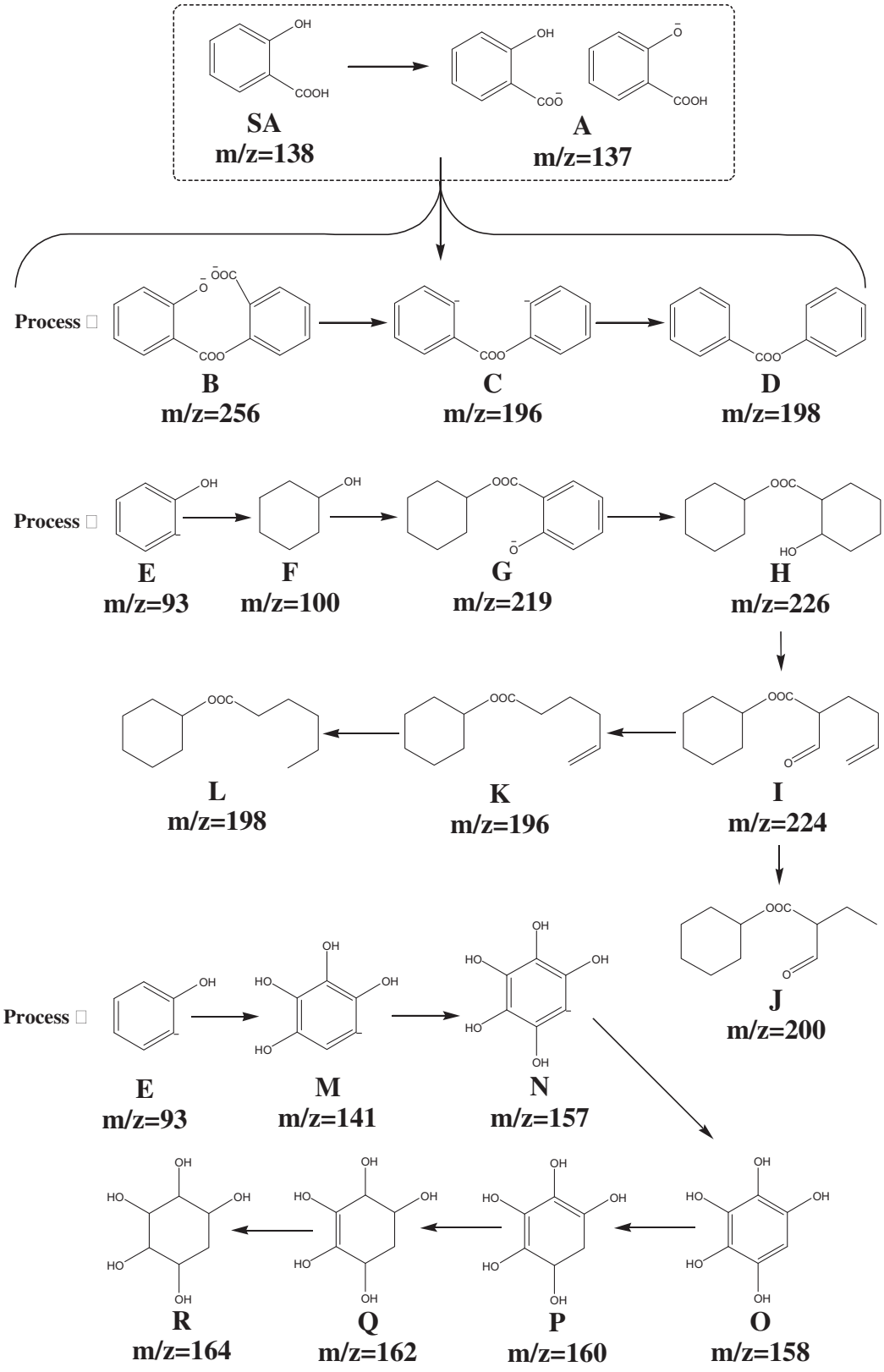

Fig. 14. The process of degradation of SA with mag-TiO_2 nanocomposites.

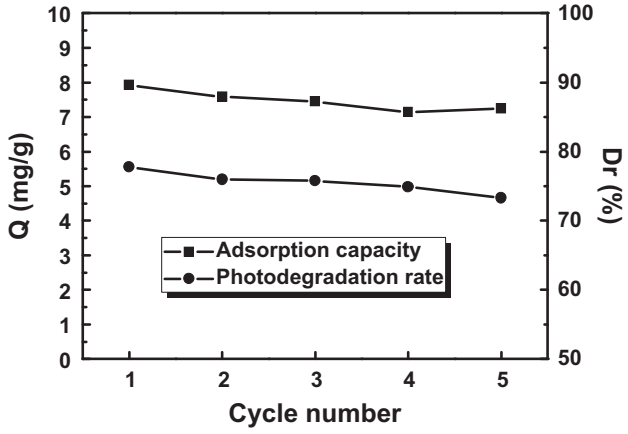

Fig. 15. Adsorption capacities of 10 mL 20 mg/L SA with 0.02 g mag-TiO_2 nanocomposites after 8 h of static dark-adsorption at 303 K in different cycles (left) and photodegradation rates of 50 mL 20 mg/L SA with 0.2 g mag-TiO_2 nanocomposites in 30 min under the visible light irradiation at 303 K in different cycles (right).

generating the intermediate product of M ($m/z = 141$) and N ($m/z = 157$), and O ($m/z = 158$) was transformed from N ($m/z = 157$), then P ($m/z = 160$), Q ($m/z = 162$) and R ($m/z = 164$) were generated from O ($m/z = 158$) by the addition reaction of hydrogen, respectively.

3.7. Stability of mag-TiO_2 nanocomposites

The stability of mag-TiO_2 nanocomposites was very important to adsorption and photodegradation of SA. To evaluate the stability of mag-TiO_2 nanocomposites, adsorption and photodegradation experiments were conducted at different conditions, which are shown in Fig. 15. Fig. 15 shows that (i) after adsorption of 10 mL 20 mg/L SA with 0.02 g mag-TiO_2 nanocomposites at 303 K, and (ii) after photodegradation of 50 mL 20 mg/L SA with 0.2 g mag-TiO_2 nanocomposites at 303 K, these samples were isolated by a magnet and sonicated with alcohol to remove the residual SA and the photocatalytic by-products, hereafter, washed with deionized water and alcohol and vacuum dried at room temperature. After five cycles, the adsorption capacities and photodegradation rates of mag-TiO_2 nanocomposites decreased very little, indicating that these as-prepared mag-TiO_2 nanocomposites had excellent chemical stability.

4. Conclusions

In this work, the mag-TiO_2 nanocomposites with good monodispersity were successfully synthesized via a mild sol–gel method, which was used for removal of SA residues. These as-prepared nanocomposites were extensively characterized by TEM, SEM, Brunauer-Emmett-Teller method, FT-IR, XRD, and VSM. The results indicated that mag-TiO_2 nanocomposites possessed the core-shell structure of good dispersibility, excellent chemical stability, magnetic property (Ms = 22.11 emu/g), and the average diameter of 290 nm. According to results of series experiments, mag-TiO_2 nanocomposites showed fast kinetics and satisfied adsorption capacity for adsorption of SA. Under the optimum experimental condition, the adsorption process followed pseudo-second-order reaction kinetics and followed the Langmuir adsorption isotherm. Moreover, the thermodynamic parameters (positive values of ΔH^o, ΔS^o and negative values of ΔG^o) calculated from the adsorption data suggested that the adsorption of SA onto mag-TiO_2 nanocomposites was a spontaneous and endothermic nature of the process. In addition, the mag-TiO_2 nanocomposites were proved to exhibit high catalytic efficiency for photodegradation of 50 mL 20 mg/L SA in 30 min under the visible light irradiation; the degradation rate could reach nearly 78% and the mineralization rate was approximately 49%. However, the mineralization rate was significantly lower than the degradation rate, indicating that there were a lot of intermediates produced during the photocatalytic process. The intermediate products were inferred from the MS.

Acknowledgments

We gratefully acknowledge the financial support of China Postdoctoral Science Foundation (No. 2012M 521015) and the Natural Science Foundation of China (No. 21207053).

References

[1] L. Khenniche, F. Aissani, Characterization and utilization of activated carbons prepared from coffee residue for adsorptive removal of salicylic acid and phenol: Kinetic and isotherm study, Desalin. Water Treat. 11 (2009) 192–203.
[2] C. Adán, J.M. Coronado, R. Bellod, J. Soria, H. Yamaoka, Photochemical and photocatalytic degradation of salicylic acid with hydrogen peroxide over TiO2/SiO2 fibres, Appl. Catal. A 303 (2006) 199–206.
[3] J.Y. Feng, X.J. Hu, P.L. Yue, Degradation of salicylic acid by photo-assisted Fenton reaction using Feions on strongly acidic ion exchange resin as catalyst, Chem. Eng. J. 100 (2004) 159–165.
[4] A.N. Rao, B. Sivasankar, V. Sadasivam, Kinetic study on the photocatalytic degradation of salicylic acid using ZnO catalyst, J. Hazard. Mater. 166 (2009) 1357–1361.
[5] S. Collado, L. Garrido, A. Laca, M. Diaz, Wet oxidation of salicylic acid solutions, Environ. Sci. Technol. 44 (2010) 8629–8635.
[6] A. Goi, Y. Veressinina, M. Trapido, Degradation of salicylic acid by Fenton and modified Fenton treatment, Chem. Eng. J. 143 (2008) 1–9.

[7] H.R. Pouretedal, S. Sabzevari, Photodegradation study of congo red, methyl orange, methyl red and methylene blue under simulated solar irradiation catalyzed by ZnS/CdS nanocomposite, Desalin. Water Treat. 28 (2011) 247–254.
[8] B.G. Lu, C.Q. Zhu, Z.X. Zhang, W. Lan, E.Q. Xie, Preparation of highly porous TiO_2 nanotubes and their catalytic applications, J. Mater. Chem. 22 (2012) 1375–1379.
[9] J. Santiago-Morales, A. Agüera, M.D.M. Gómez, A.R. Fernández-Alba, J. Giménez, S. Esplugas, R. Rosal, Transformation products and reaction kinetics in simulated solar light photocatalytic degradation of propranolol using Ce-doped TiO2, Appl. Catal. B 129 (2013) 13–29.
[10] Z.Y. Lu, W.C. Zhou, P.W. Huo, Y.Y. Luo, M. He, J.M. Pan, C. X. Li, Y.S. Yan, Performance of a novel TiO_2 photocatalyst based on the magnetic floating fly-ash cenospheres for the purpose of treating waste by waste, Chem. Eng. J. 225 (2013) 34–42.
[11] D.L. Zhao, G.D. Sheng, C.L. Chen, X.K. Wang, Enhanced photocatalytic degradation of methylene blue under visible irradiation on graphene@TiO_2 dyade structure, Appl. Catal. B 111–112 (2012) 303–308.
[12] O.E. Kartal, G.D. Turhan, Decolourization of C.I. reactive orange 16 via photocatalysis involving TiO_2/UV and TiO_2/UV/oxidant systems, Desalin. Water Treat. 48 (2012) 199–208.
[13] W. Guan, J.M. Pan, H.X. Ou, X. Wang, X.H. Zou, W. Hua, C. X. Li, X.Y. Wu, Removal of strontium(II) ions by potassium tetratitanate whisker and sodium trititanate whisker from aqueous solution: Equilibrium, kinetics and thermodynamics, Chem. Eng. J. 167 (2011) 215–222.
[14] L. Khenniche, F. Aissani, Preparation and characterization of carbons from coffee residue: Adsorption of salicylic acid on the prepared carbons, J. Chem. Eng. Data 55 (2010) 728–734.
[15] J.M. Pan, W. Hu, X.H. Dai, W. Guan, X.H. Zou, X. Wang, P.W. Huo, Y.S. Yan, Molecularly imprinted polymers based on magnetic fly-ash-cenosphere composites for bisphenol A recognition, J. Mater. Chem. 21 (2011) 15741–15751.
[16] X.B. Luo, Y.C. Zhan, Y.N. Huang, L.X. Yang, X.M. Tu, S.L. Luo, Removal of water-soluble acid dyes from water environment using a novel magnetic molecularly imprinted polymer, J. Hazard. Mater. 187 (2011) 274–282.
[17] A.R. Contreras, A. Garcia, E. Gonzalez, E. Casals, V. Punte, A. Sanchez, X. Font, S. Recillas, Potential use of CeO_2, TiO_2 and Fe_3O_4 nanoparticles for the removal of cadmium from water, Desalin. Water Treat. 41 (2012) 296–300.
[18] J.R. Meng, C.Y. Shi, B.W. Wei, W.J. Yu, C.H. Deng, X.M. Zhang, Preparation of Fe_3O_4@C@PANI magnetic microspheres for the extraction and analysis of phenolic compounds in water samples by gas chromatograph-mass spectrometry, J. Chromatogr. A 1218 (2011) 2841–2847.
[19] D.K. Yi, S.S. Lee, J.Y. Ying, Synthesis and applications of magnetic nanocomposite catalysts, Chem. Mater. 18 (2006) 2459–2461.
[20] M.A.M. Gijs, F. Lacharme, U. Lehmann, Microfluidic applications of magnetic particles for biological analysis and catalysis, Chem. Rev. 110 (2010) 1518–1563.
[21] D.N. Bui, S.Z. Kang, X.Q. Li, J. Mu, Effect of Si doping on the photocatalytic activity and photoelectrochemical property of TiO_2 nanoparticles, Chem. Commun. 13 (2011) 14–17.
[22] L.C. Xu, J.D. Dai, J.M. Pan, X.X. Li, P.W. Huo, Y.S. Yan, X.B. Zou, R.X. Zhang, Performance of rattle-type magnetic mesoporous silica spheres in the adsorption of single and binary antibiotics, Chem. Eng. J. 174 (2011) 221–230.
[23] W. Zhang, L. Qin, X.W. He, W.Y. Li, Y.K. Zhang, Novel surface modified molecularly imprinted polymer using acryloyl-β-cyclodextrin and acrylamide as monomers for selective recognition of lysozyme in aqueous solution, J. Chromatogr. A 1216 (2009) 4560–4567.
[24] S.S. Gupta, K.G. Bhattacharyya, Interaction of metal ions with clays. I. A case study with Pb(II), Appl. Clay Sci. 30 (2005) 199–208.
[25] M. Sathishkumar, A.R. Binupriya, D. Kavitha, R. Selvakumar, R. Jayabalan, J.G. Choi, S.E. Yun, Adsorption potential of maize cob carbon for 2,4-dichlorophenol removal from aqueous solutions: Equilibrium, kinetics and thermodynamics modeling, Chem. Eng. J. 147 (2009) 265–271.
[26] J.M. Pan, H. Yao, W. Guan, H.X. Ou, P.W. Huo, X. Wang, X.H. Zou, C.X. Li, Selective adsorption of 2,6-dichlorophenol by surface imprinted polymers using polyaniline/silica gel composites as functional support: Equilibrium, kinetics, thermodynamics modeling, Chem. Eng. J. 172 (2011) 847–855.
[27] O. Aksakal, H. Ucun, Equilibrium, kinetic and thermodynamic studies of the biosorption of textile dye (Reactive Red 195) onto *Pinus sylvestris* L, J. Hazard. Mater. 181 (2010) 666–672.
[28] Y.S. Ho, G. McKay, Pseudo-second order model for sorption processes, Process Biochem. 34 (1999) 451–465.
[29] Z.J. Wu, H. Joo, K. Lee, Kinetics and thermodynamics of the organic dye adsorption on the mesoporous hybrid xerogel, Chem. Eng. J. 112 (2005) 227–236.
[30] G. Baydemir, M. Andac, N. Bereli, R. Say, A. Denizli, Selective removal of bilirubin from human plasma with bilirubin-imprinted particles, Ind. Eng. Chem. Res. 46 (2007) 2843–2852.
[31] M. Mazzotti, Equilibrium theory based design of simulated moving bed precesses for a generalized Langmuir isotherm, J. Chromatogr. A 1126 (2006) 311–322.
[32] K.Q. Li, X.H. Wang, Adsorptive removal of Pb(II) by activated carbon prepared from *Spartina alterniflora*: Equilibrium, kinetics and thermodynamics, Bioresour. Technol. 100 (2009) 2810–2815.
[33] M. Tuzen, D. Citak, M. Soylak, 5-Chloro-2-hydroxyaniline-copper(II) coprecipitation system for preconcentration and separation of lead(II) and chromium(III) at trace levels, J. Hazard. Mater. 158 (2008) 137–141.